Microchemical Journal 210 (2025) 112956

Contents lists available at ScienceDirect

Microchemical Journal

journal homepage: www.elsevier.com/locate/microc

Improved sampling strategy for high-performance materials: The introduction of the stethoscope cell for online-LASIL experiments

Maximilian Podsednik [a,b], Maximilian Weiss [a], Johannes Frank [a], Erwin Peck [c], Silvia Larisegger [b], Helmut Riedl [c,d], Paul H. Mayrhofer [c], Andreas Limbeck [a,*]

[a] TU Wien, Institute of Chemical Technologies and Analytics, Getreidemarkt 9/164-I2AC 1060 Vienna, Austria
[b] KAI Kompetenzzentrum Automobil- und Industrieelektronik GmbH, Argentinierstraße 8 1040 Wien, Austria
[c] TU Wien, Institute of Materials Science and Technology, Getreidemarkt 9/E308 1060 Vienna, Austria
[d] TU Wien, Christian Doppler Laboratory for Surface Engineering of High-performance Components, Austria

ARTICLE INFO

Keywords:
Online-LASIL cell design
Stethoscope cell
Quantitative analysis

ABSTRACT

The development and optimization of high-performance materials, which are crucial for efficient and sustainable technologies, require a precise quantitative analysis of their bulk composition. Online-laser ablation of solids in liquids (online-LASIL) combined with an ICP-MS detection is a method that allows simple determination of the elemental composition with commercially available liquid standards and avoids error-prone digestion of the sample. To overcome the limitations in the analysis of samples with varying geometries, the stethoscope cell was introduced to eliminate the problems of previous designs. In this work, the analytical performance of the stethoscope cell is demonstrated, enabling the analysis of samples with dimensions ranging between 7 and 20 mm and sample thicknesses up to 10 mm. Two application examples further show the achieved improvements using the stethoscope cell: A quantitative bulk measurement of an industrial TiW-sputter target and a depth-resolved analysis of protective coatings deposited on steel substrates. The analysis demonstrates the quantification of main and minor components within the samples with a measurement reproducibility varying between <1–10 %RSD depending on the concentration. To validate the results of the new cell design, acid digestions with a subsequent ICP-OES measurement were performed. Both online-LASIL measurements show a good agreement with the ICP-OES reference measurements, confirming the suitability of the stethoscope cell for quantitative and depth-resolved online-LASIL experiments.

1. Introduction

The increasing CO_2 emission of the world's population is posing one of the major challenges of the 21st century. The effects of climate change are noticeable around the globe, with a rising occurrence of extreme weather conditions [1]. To overcome this challenge, it is mandatory to develop more efficient technologies and expand renewable energy sources, resulting in a demand for new materials with improved properties [2]. For that reason, material development and design play a vital role in overcoming the challenges of the 21st century. For the optimization of novel materials and to locate errors in the production processes, a precise chemical analysis of the sample composition is essential. Besides sample stoichiometry, obtaining quantitative information about additives or unwanted contaminants is also necessary for suitable process control.

A conventional solution for that challenge would be the digestion of the sample and subsequent liquid analysis of the resulting sample solution using, e.g., inductively coupled plasma–mass spectrometry [3], or optical emission spectroscopy [4] (ICP-MS or ICP-OES), atomic absorption spectroscopy [5] (AAS). However, many novel high-performing materials, like protective [6,7], or thermal barrier coatings [8,9], are hard-to-digest materials, thus requiring, besides harsh conditions, corrosive or potentially harmful chemicals like HF or sample fusion. Moreover, considering thin protective coatings, the digestion of the whole system is often not advisable since the comparatively high mass of the substrate could lead to interferences in the analysis or unwanted contaminations, and selective dissolution of the coating is often not feasible.

To overcome the problems associated with sample digestion, the analysis of the solid material is recommended. Frequently applied solid

* Corresponding author.
E-mail address: andreas.limbeck@tuwien.ac.at (A. Limbeck).

https://doi.org/10.1016/j.microc.2025.112956
Received 30 October 2024; Received in revised form 27 January 2025; Accepted 2 February 2025
Available online 5 February 2025
0026-265X/© 2025 The Authors. Published by Elsevier B.V. This is an open access article under the CC BY license (http://creativecommons.org/licenses/by/4.0/).

sampling techniques include methods such as laser ablation inductively plasma mass spectrometry [10,11] (LA-ICP-MS), laser-induced breakdown spectroscopy [12,13] (LIBS), secondary ion mass spectrometry [14,15] (SIMS), glow discharge-mass spectrometry [16] or optical emission spectroscopy [17] (GD-MS or GD-OES), or X-ray fluorescence spectroscopy (XRF). These methods allow simple analysis of chemically inert materials and enable spatially resolved analysis to differentiate between coating and substrate. However, for an accurate quantitative analysis, the mentioned methods require matrix-matched standards or certified reference materials, often unavailable for novel high-performance materials [18].

Another approach that recently demonstrated its effectiveness in spatially resolved analysis of solid materials is online-laser ablation of solids in liquids (LASIL) [19–21]. In online-LASIL, the sample is ablated into a continuously flowing carrier solution using a laser system. The liquid flow over the sample is achieved by an in-house built online-LASIL cell. As demonstrated by Muravitskaya et al. [22], the nanoparticles generated by the laser ablation of the sample behave like dissolved ions when introduced into an ICP-MS. For this reason, online-LASIL does not depend on certified reference materials or matrix-matched standards and can use commercially available liquid standards for quantification. This enables the economical and quick adaptation of online-LASIL experiments for novel, hard-to-digest materials. Looking at the online-LASIL cell design introduced by Bonta et al. [19], it becomes evident that the cavity used for the sample was optimized for sample geometries of 5×5 mm^2 and a height of 0.5 mm. This setup also allows the analysis of smaller samples, even though the analytical performance might be reduced due to changed flow dynamics, especially for very thin samples. However, bigger samples must be fragmented to fit the size of the LASIL cell, adding additional sample preparation and increasing the risk of contamination.

This limitation of the online-LASIL cell design is addressed in this work. To conduct online-LASIL experiments without being restricted by the sample's geometry, the stethoscope cell is introduced. As the name already implies, the stethoscope cell is placed on top of the sample, enabling the analysis of samples at least 7 mm in length, and the sample thickness is mainly limited by the length of the screws used to seal the cell. To demonstrate the capabilities of the new cell design, the composition of an industrial TiW sputter target with a diameter of 450 mm was evaluated. Additionally, the applicability of the stethoscope cell is demonstrated by the analysis of boride coatings deposited on steel substrates. Those protective coatings, with their high hardness and self-lubricating properties [7,23], are responsible for increasing the efficiency of components essential for industrial manufacturing [24].

2. Experimental

2.1. Reagents and samples

All solutions and dilutions were prepared freshly with deionized water (18.2 MΩcm^{-1}) from a Barnstead EASYPURE II water dispenser (ThermoFisher Scientific, Germany). The concentrated acids nitric acid (HNO_3) and hydrofluoric acid (HF), chemicals or the ICP standards were at least in analytical quality and purchased from VWR International (USA). The ICP standards of B, Mg, Al, Ti, W, and In had a concentration of 1000 mg/kg. The gases used for the operation of the ICP-MS and ICP-OES, Ar as plasma gas and He as collision gas, had a purity of 5.0 and were purchased from Messer Austria (Gumpoldskirchen, Austria).

The industrial TiW-sputter target, which had a diameter of 450 mm, was manufactured by Honeywell (USA). For the analysis, the sputter target was machined into $10 \times 10 \times 2$ mm^3 pieces since the whole target was not suitable for the stethoscope cell (see Fig. 1). For the liquid ICP-OES measurements, the samples were broken into pieces with dimensions of approximately 1–2 mm in diameter, corresponding to a mass of ~0.2 g. All pieces were cleaned for 15 min with deionized water in an ultrasonic bath to avoid contamination from the cutting process.

The $AlMgB_{14}$ and $AlMgB_{14} + TiB_2$ protective coatings were deposited on different substrates, including austenitic steel ($20 \times 7 \times 1$ mm^3) and 11-02-oriented sapphire ($10 \times 10 \times 0.53$ mm^3) using DC magnetron sputtering in a modified Leybold Heraeus Z400 coating system. For the $AlMgB_{14}$ coating, a single powder metallurgically produced stoichiometric target was used and the temperature of the substrate was varied between 300 and 600 °C in steps of 100 °C. The TiB_2 for the $AlMB_{14} + TiB_2$ coating was alloyed by placing $2 \times 2 \times 2$ mm^3 pieces of TiB_2 on the racetrack of the $AlMgB_{14}$ target. To investigate the influence of the TiB_2 content on $AlMgB_{14}$, three coatings with 8, 12, and 16 TiB_2 pieces were synthesized. For all coatings, a face-to-face configuration of target and substrate with a distance of 40 mm was chosen. The base pressure before each deposition was below 0.5 mPa. As a working gas for the sputtering process, argon with a flow rate of 35 sccm was used, leading to a process pressure of 0.40–0.43 Pa. A constant target current of 0.75 A was used, resulting in a power density of approximately 9.7 W/cm^2.The deposition time was 60 min, resulting in coating thicknesses of approximately 3 μm. The labeling and the deposition parameters of the two sample series can be seen in Table S1.

2.2. Online-LASIL measurement setup

The samples were ablated using a commercially available LIBS system, the J200 Tandem LA/LIBS (Applied Spectra Inc., Fermont, CA), with a 266 nm wavelength and a pulse width of four ns. For the analysis, the online-LASIL cell is placed in the sample stage of the system, offering the recording of spatially resolved information [25,26]. Therefore, the cell can be universally used in laser systems from different

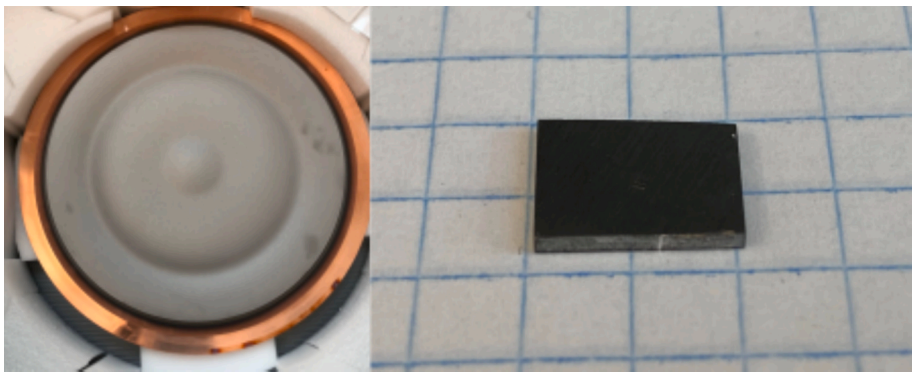

Fig. 1. Picture of the analyzed TiW-sputter target (left) and the machined sample for the online-LASIL analysis (right).

manufacturers. The only limiting factor is the geometry of the ablation chamber, which needs to be large enough to fit the cell and the connected tubing. To maximize the setup's washout behavior, a controlled segmentation of the carrier was employed, using a six-port-valve controlled by an Arduino controller [27]. The segmentation of the carrier solution was achieved by releasing Ar-gas every 10 s for 0.3 s with a pressure of approximately 0.8 bar.

An iCAP TQ ICP-MS from (Thermo Fisher Scientific, Germany) was used as a detection system in kinetic energy discrimination (KED) mode using He as KED-gas. The nanoparticle suspension generated in the LASIL process was introduced into the ICP-MS using a PFA nebulizer and a cyclonic spray chamber. The overall flow rate of the sample introduction was 1.6 ml/min, consisting of 1.1 ml/min of the carrier solution, spiked with 1 ng/g In as an internal standard and 0.5 ml/min of the make-up solution. For the analysis of the TiW-sputter target, an HF-resistant sample introduction kit consisting of a PFA cyclonic spray chamber and a sapphire torch was used since diluted HF was used as a make-up solution. Before all experiments, the ICP-MS was tuned for the maximum intensity of the ^{115}In signal and a CeO^+/Ce^+ ratio below 2 % using a solution from the manufacturer. Finally, the instrument software Qtegra Version 2.10 recorded and analyzed the data. The detailed laser and ICP-MS parameters are listed in Table 1.

2.3. Reference ICP-OES measurements

Liquid ICP-OES measurements were conducted to obtain reference values for both online-LASIL experiments. The approximately 0.2 g TiW-sputter target fragments were used for the analysis. Three samples were digested by a mixture of 1 ml HNO_3 and 1 ml HF for 10 min at room temperature. For the reference measurements of the protective coatings, the coatings of interest were deposited on sapphire substrates, unaffected by the digestion parameters. The samples were broken into pieces with dimensions of approximately 5x5 mm^2. For the digestion of the coatings, a mixture of 0.25 ml HNO_3 and 0.25 ml HF for 30 min at 100 °C was used. After the samples cooled to room temperature, they were diluted to 40 ml and spiked with 1 µg/g Eu as the internal standard. Due to the higher sample intake of the TiW-sputter target, a second dilution by a factor of 100 was needed.

Table 1
ICP-MS and laser parameters of the online-LASIL measurements.

ICP-MS detection system		
Parameter	**Value**	
RF Power	1550 W	
Nebulizer gas flow	1.02 l/min	
Cool gas flow	14 l/min	
Auxiliary gas flow	0.8 l/min	
KED gas flow (He)	3.5 ml/min	
CCT bias	−21 V	
Pole bias	−18 V	
Measured Isotopes	**TiW-sputter target**	**Protective coatings**
	^{46}Ti, ^{47}Ti, ^{48}Ti, ^{50}Ti, ^{115}In, ^{182}W, ^{183}W, ^{184}W, and ^{186}W	^{10}B, ^{11}B, ^{24}Mg, ^{25}Mg, ^{27}Al, ^{46}Ti, ^{47}Ti, ^{48}Ti, ^{50}Ti, ^{57}Fe and ^{115}In
Dwell time	0.01 s	
Laser		
Parameter	**Value**	
Laser fluence	12 J/cm^2	
Spot size	100 µm	
Scan speed	0.5 mm/s	
Repetition rate	20 Hz	

For the analysis, a Thermo iCAP 6500 ICP-OES (ThermoFisher Scientific, Germany), equipped with an HF-resistant sample introduction kit, was used as a detection system. The sample introduction was accomplished using an ASX-520 autosampler (CETAC Technologies, USA), a PTFE concentric nebulizer, a PTFE cyclonic spray chamber, and a ceramic injector tube. The detailed ICP-OES parameters can be seen in Table S2). The obtained emission signals were quantified with an external calibration using liquid ICP standards. Two emission lines per element were monitored for quantification, and the instrument software Qtegra (Version 2.8) was used to evaluate the data.

3. Results and discussion

3.1. Analytical performance of the stethoscope cell

As mentioned in the introduction, the old cell design did not only limit the analyzable samples' width and length but also their height, as the cell was optimized for standardized substrates with a thickness of 0.5 mm. Therefore, thicker samples could not be analyzed without time-consuming thinning to fulfill this precondition, and thinner samples had to be fixated to prevent the sample from moving during the analysis. The new cell design avoids all those disadvantages by using it like a stethoscope, making it easily adaptable to varying sample geometries (size and thickness).

The assembled stethoscope cell is illustrated in Fig. 2; it consists of three components machined out of polyether ether ketone (PEEK): the top part, the bottom part, and the actual stethoscope cell. The top and bottom parts are primarily needed to achieve a sealed flow of the carrier solution over the sample. To apply pressure, four bolts are screwed into the threads of the bottom part. Within the stethoscope cell, seven holes are drilled, with the outer four serving as guides to position the cell on the sample. The two drillings in the middle are equipped with PTFE tubes (outer diameter: 1.6 mm), enabling the introduction of the carrier solution. A quartz glass is placed in the cavity in the middle of the cell, allowing the ablation of the sample through a 1.5 × 4 mm^2 window. Two PDMS films with channels are used to avoid leakages between the sample, the cell, and the quartz glass. Besides the sealing of the cell, the PDMS foil between the sample and the stethoscope cell enables the flow of the carrier solution over the sample. Comparable to the old design, the continuous flow of the carrier solution was achieved using a peristaltic pump (Perimax 12, SPETEC, Germany).

While this new design offers more flexibility regarding the sample's geometry, there are still limitations remaining, like at least one flat surface for the analysis, a minimum sample size of 7 mm, and a maximal sample width, which is limited by the length of the four screws used for sealing the cell. The minimum size request is crucial to realize a sealed flow of the carrier solution over the sample, given by the distance of the inlet and outlet of the carrier solution. Moreover, due to the redesign, there is a slightly larger dead volume between the sample and the silica glass (cf. Fig. 2), which is necessary to ensure the stability of the stethoscope cell. Because of this increased volume, a higher flow of the carrier solution (1.6 ml/min) is necessary to ensure a sufficiently fast sample washout. While this leads to decreased analysis times, it also results in a higher dilution of the ablated material and, thus, overall, a slightly reduced sensitivity. Nonetheless, the flexibility gained to quickly adapt the measurements setup for varying sample geometries, especially their thickness, outweighs those limitations for the following applications.

3.2. Quantitative bulk analysis of an industrial sputter target

To demonstrate the quick adaptation of the stethoscope cell to different materials and applications, a roughly 10x10x2 mm^3 piece of an industrial TiW-sputter target, prepared as explained in chapter 2.1, was analyzed. The analysis of the sputter target composition is ideally suited to demonstrate the advantages of the stethoscope cell. In contrast, with

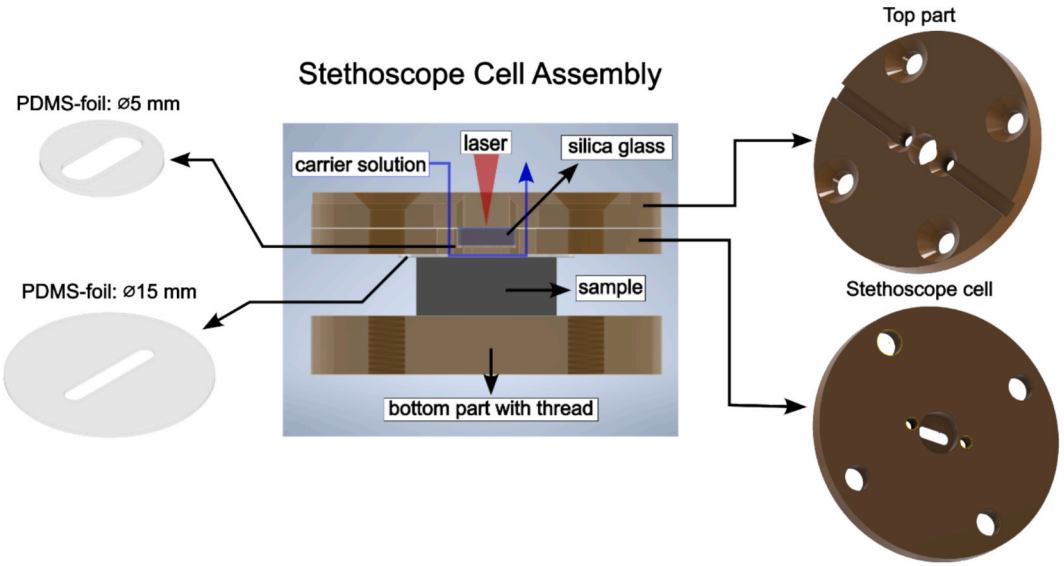

Fig. 2. Detailed depiction of the stethoscope cell assembly, including a cross-section and the models of the "top part," the "stethoscope cell," and the two PDMS foils with 5 and 15 mm diameters.

the old cell design, the sample would have needed to be machined to fit precisely into the 5 × 5 × 0.5 mm^3 cavity. This would add time for sample preparation and increase the risk of contamination. At this point, it is worth mentioning that even for the conventional liquid ICP-OES analysis, additional time was needed since the preparation of a smaller piece was necessary to avoid large amounts of concentrated acids for complete sample dissolution since HF is required to digest the TiW-sputter target.

For this online-LASIL experiment, a 0.6 mol/l NaF buffer solution with a pH of 6, acidified with concentrated HF, was used as a carrier solution. The buffer was chosen since, according to the literature [28], HF is required to stabilize W in an aqueous solution. However, adding HF to the carrier solution was not feasible as even diluted HF slightly etched the sputter target, resulting in elevated and unstable background signals. After sample ablation, a make-up solution, consisting of a mixture of 5 % (v/v) HNO_3 and 1 % (v/v) HF, was introduced via a T-piece connected with a 30 mm PTFE-tubing to the outlet of the cell, enabling transport of the ablated material to the ICP-MS without significant losses.

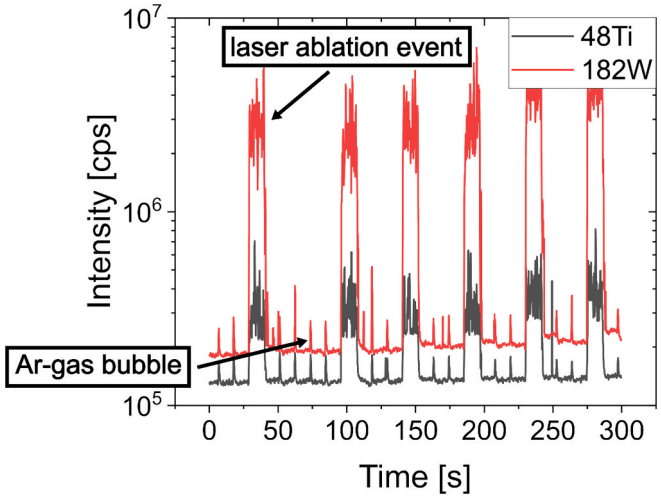

Fig. 3. Washout behavior of the ablated TiW-sputter target using the stethoscope cell and a controlled segmentation of the carrier solution. One can see six ablation events resulting from line scans and small peaks, which reoccur every 10 s due to the introduced Ar-gas bubbles.

The transient signal of the ablated TiW-sample can be seen in Fig. 3. Besides the ablation events of six laser lines, small, reoccurring peaks can also be seen, resulting from the Ar-bubbles introduced to segment the carrier solution. For the data analysis, the signal caused by the Ar-bubbles was not considered. In this experiment, every 10 s an Ar-bubble was introduced into the carrier solution. Looking at the washout time of the ablation events, it becomes evident that the material generated in the ablation process is completely washed out within one liquid segment. This demonstrated that the combination of the new cell design and the controlled segmentation of the carrier solutions results in washout behaviors comparable to those of the old design, even when using the T-piece. As stated by Podsednik et al. [27], the washout time is mainly limited by the synchronization of the laser pattern with the liquid segments.

For sample analysis, line scans with the parameters listed in Table 2 were performed, while a pre-ablation of the sample was conducted to avoid contaminations on the surface. The online-LASIL analysis was performed on a single sample, which was analyzed with six 2 mm long laser patterns. For the quantification of the online-LASIL measurements (n = 6), a standard addition method, as described by Herzig et al. [22], was utilized, resulting in a composition of 68.1 % ± 3.5 % for W and 31.9 % ± 3.5 % for Ti.

To evaluate the results of the online-LASIL analysis using the stethoscope cell as a sampling device, conventional liquid ICP-OES measurements were conducted as a reference. For the ICP-OES measurements, three 1–2 mm fragments of the target were digested. ICP-OES analysis of the derived sample solutions (n = 3) indicated a composition of 70.4 % ± 0.5 % for W and 29.6 % ± 0.5 % for Ti, showing no significant deviation from the online-LASIL analysis. However, the relative standard deviation for online-LASIL is higher, at 10 % for Ti and 5 % for W, compared to the 2 % for ICP-OES measurements. Looking at the analysis time, the online-LASIL method is more efficient since the samples' digestion and additional machining steps for the small fragments can be avoided. Moreover, the distinct advantage of online-LASIL for this type of sample, besides time efficiency, is its ability to prevent the use of corrosive and toxic acids, which is in accordance with the principles of green analytical chemistry [29,30].

3.3. *Quantitative depth-resolved analysis of protective coatings*

To further demonstrate the great flexibility of the new stethoscope

Table 2
Results of the online-LASIL measurements of the protective coatings deposited on steel (n = 10) compared to the ICP-OES measurements of the digested coatings deposited on sapphire (n = 3). This table provides information about the mean composition of the coatings and the reproducibility of the measurement (average ± standard deviation).

	Online-LASIL				ICP-OES			
	B at%	Mg at%	Al at%	Ti at%	B at%	Mg at%	Al at%	Ti at%
A	90.54 % ± 0.55 %	0.53 % ± 0.04 %	5.33 % ± 0.33 %	3.60 % ± 0.28 %	89.32 % ± 0.59 %	0.25 % ± 0.04 %	5.53 % ± 0.06 %	4.91 % ± 0.05 %
B	88.74 % ± 0.32 %	0.66 % ± 0.05 %	5.04 % ± 0.28 %	5.55 % ± 0.25 %	88.22 % ± 0.81 %	0.46 % ± 0.03 %	4.85 % ± 0.11 %	6.47 % ± 0.05 %
C	88.01 % ± 1.03 %	1.12 ± 0.09 %	4.50 % ± 0.33 %	6.37 % ± 0.96 %	86.82 % ± 0.54 %	0.53 % ± 0.03 %	4.53 % ± 0.02 %	8.12 % ± 0.06 %
D	86.14 % ± 1.71 %	6.28 % ± 1.01 %	7.58 % ± 0.74 %	/	83.57 % ± 1.07 %	7.58 % ± 0.32 %	8.68 % ± 0.22 %	/
E	86.56 % ± 1.01 %	5.86 % ± 0.63 %	7.58 % ± 0.56 %	/	90.52 % ± 1.40 %	3.10 % ± 0.03 %	6.20 % ± 0.06 %	/
F	89.27 % ± 0.99 %	3.20 % ± 0.47 %	7.53 % ± 0.65 %	/	/	/	/	/
G	89.25 % ± 0.75 %	2.66 % ± 0.26 %	8.09 % ± 0.58 %	/	88.75 % ± 1.57 %	3.61 % ± 0.04 %	7.43 % ± 0.41 %	/

cell, $AlMgB_{14}$ and $AlMgB_{14}$ + TiB_2 coating on steel substrates were analyzed. These superhard, self-lubricating protective coatings improve rotational and sliding components' wear resistance and friction. Therefore, they are ideal for application in motors and hydraulic pumps, leading to a 10 % increase in efficiency [24]. However, especially to achieve the required hardness of coatings deposited by magnetron sputtering, the crystallinity of the $AlMgB_{14}$ films is crucial. So far, this crystallization has only been achieved with pulsed laser deposition (PLD) [23]. Two approaches have been executed to achieve crystalline coatings using magnetron sputtering. Firstly, TiB_2 was alloyed and sputtered, and secondly, the $AlMgB_{14}$ coatings were deposited on the substrate at elevated temperatures. To manufacture those thin films, a stoichiometric deposition of the boride coatings is essential to guarantee their mechanical properties. Thus, a quick quantitative analysis is mandatory to optimize deposition parameters or detect errors [31].

However, the high chemical inertness must be considered for conventional digestion of the coatings with a subsequent liquid measurement. Thus, harsh conditions are required for complete dissolution. Therefore, a simultaneous digestion of the steel substrate cannot be avoided. Considering the high mass of the steel substrate (10 mm thickness) compared to the protective coatings (3 μm thickness), even trace contaminations can impact the quantification of the coating's composition. On the other hand, solid sampling methods like LA-ICP-MS, ToF-SIMS, EDX, or LIBS could be used to measure the coating without being influenced by the steel substrate. However, those solid sampling techniques are either dependent on matrix-matched standards or, in the case of EDX, they are not suited for analyzing light elements like B [32]. Therefore, online-LASIL using the stethoscope cell is the ideal analytical method since neither matrix-matched standards nor additional sample preparation is needed, and the required spatial resolution to solely ablate the coating is provided.

For an optimized transport of the ablated material to the ICP-MS, a 0.9 mol/l NH_4Cl solution was adjusted to a pH of 5 using concentrated HCl. To further stabilize the nanoparticle suspension generated in the ablation process, a 3 % (v/v) HCl was introduced via the t-piece after the outlet of the stethoscope cell. For the online-LASIL measurements, ten line scans (each with a length of 2 mm) were performed per sample using the laser parameters described in Table 1. The laser parameters resulted in a mean ablation rate of approximately 500 nm per ablated line, allowing six ablation layers before reaching the steel substrate. To estimate differences in the thickness of the protective coatings, the ^{57}Fe isotope was also measured; additionally, a pre-ablation of the surface was conducted using the same laser parameters to avoid surface contaminations. For the quantification of the results, the same standard addition method as used for the TiW-sputter target has been applied; the results are presented in Table 2. Additionally, acid digestion of the coatings, followed by ICP-OES measurements, was conducted to verify the online-LASIL method. However, due to the risk of contamination by concurrent dissolution of the steel substrate, the coatings were deposited on sapphire. Consequently, the coatings could be digested without dissolving the substrate using a mixture of HNO_3 and HF. The results of the ICP-OES analysis are listed in Table 2; sample F could not be analyzed due to an incomplete digestion.

The comparison of the results in Table 2 shows a great agreement for the B content, while slight deviations exist for the other analyzed elements. It is assumed that the deviation of the measurements can be attributed to several causes. Firstly, the coatings were deposited on different types of substrates. Furthermore, the sampling volume of the methods cannot be compared, as the ICP-OES measurements analyzed a 5 × 5 mm^2 area. In contrast, ten lines with a beam diameter of 100 μm were ablated in the online LASIL measurements. Therefore, the deviation can also indicate inhomogeneities within the sample. However, both measurements show the same trends within the sample series.

Upon further examination of the coating composition, conducting online-LASIL experiments with the stethoscope cell provides quick insight into the effects of the sputtering parameters. The results show that Ti is incorporated when adding TiB_2 pieces for magnetron sputtering. Additionally, the Ti content increases with the amount of Ti pieces used for the deposition. Furthermore, the measurements indicate that depositing pure $AlMgB_{14}$ on heated substrates leads to the loss of Magnesium, resulting in a non-stoichiometric deposition. It is expected that the Magnesium vaporizes as its content decreases with temperature. This experiment demonstrates that the stethoscope cell enables reliable quantification while further minimizing the sample preparation. This is especially helpful for coatings deposited on varying substrates, as, besides a stoichiometric deposition, the adhesion of the coatings to the substrate is also a crucial parameter [33]. Therefore, due to its geometry-independent sampling, the stethoscope cell eliminates additional deposition on analyzable substrates.

4. Conclusion

In recent years, online-LASIL has been successfully used to analyze various materials. However, restrictions in the required sample geometry prevented a more general application. To establish online-LASIL for a broader sample selection, this work developed a new online-LASIL cell design, which is used comparable to a stethoscope. The redesign enables the analysis of samples at least 7 mm in length, and the thickness of the samples is only limited by the length of the screws used to seal the cell. Therefore, the stethoscope cell easily adapts to varying sample geometries, guarantees a perfect fit, and minimizes sample preparation. Consequently, the stethoscope cell represents a start toward enabling geometry-independent sampling in online-LASIL experiments.

The applicability of the stethoscope cell has been shown for the analysis of a TiW-sputter target and protective coatings. Both measurements reflect the advantages of the new design by comparing the differing geometries of the TiW-sputter target (10 × 10 × 1 mm^3) and the protective coatings (20 × 7 × 1 mm^3). Neither sample would have

been analyzable without additional sample preparation using the old cell design. While the analysis of the TiW-sputter target provides a quantitative assessment of the bulk composition, the measurements of the protective coating illustrate a depth-resolved application, enabling a clear differentiation between the substrate and applied coating.

The current operation of the stethoscope cell requires increased flow speed to flush the volume over the sample, which results in an overall reduction in sensitivity. However, this issue is of minor importance in the shown application examples because only the main components were examined. Further improvements will be focused on reducing the cells' dead volume to enable fast washouts with reduced flow rates.

CRediT authorship contribution statement

Maximilian Podsednik: Writing – original draft, Visualization, Validation, Methodology, Investigation, Data curation, Conceptualization. **Maximilian Weiss:** Methodology, Conceptualization. **Johannes Frank:** Methodology, Conceptualization. **Erwin Peck:** Methodology, Conceptualization. **Silvia Larisegger:** Project administration, Funding acquisition. **Helmut Riedl:** Resources, Conceptualization. **Paul H. Mayrhofer:** Writing – review & editing, Resources, Methodology. **Andreas Limbeck:** Validation, Supervision, Resources, Project administration, Funding acquisition, Conceptualization.

Declaration of competing interest

The authors declare that they have no known competing financial interests or personal relationships that could have appeared to influence the work reported in this paper.

Acknowledgements

This work was funded by the Austrian Research Promotion Agency (FFG, Project No. 884573/898207/905107). The authors acknowledge TU Wien Bibliothek for financial support through its Open Access Funding Program.

The financial support by the Austrian Federal Ministry for Digital and Economic Affairs, the National Foundation for Research, Technology, and Development, and the Christian Doppler Research Association is gratefully acknowledged (Christian Doppler Laboratory "Surface Engineering of high-performance Components").

Appendix A. Supplementary data

Supplementary data to this article can be found online at https://doi.org/10.1016/j.microc.2025.112956.

Data availability

Data will be made available on request.

References

[1] K.L. Ebi, J. Vanos, J.W. Baldwin, J.E. Bell, D.M. Hondula, N.A. Errett, K. Hayes, C. E. Reid, S. Saha, J. Spector, P. Berry, Extreme weather and climate change: population health and health system implications, Annu. Rev. Public Health 42 (2021) 293–315, https://doi.org/10.1146/annurev-publhealth-012420-105026.

[2] W.L. Zheng, N.H. Tien, A. Sibghatullah, D. Asih, M. Soelton, Y. Ramli, Impact of energy efficiency, technology innovation, institutional quality, and trade openness on greenhouse gas emissions in ten Asian economies, Environ. Sci. Pollut. Res. 30 (2023) 43024–43039, https://doi.org/10.1007/s11356-022-20079-3.

[3] C.M. Senger, K.F. Anschau, L. Baumann, A.L.H. Muller, P.A. Mello, E.I. Muller, Eco-friendly sample preparation method for silicon carbide using pyrohydrolysis for subsequent determination of tungsten by ICP-MS, Microchem. J. 171 (2021), https://doi.org/10.1016/j.microc.2021.106781.

[4] C. Morrison, H.C. Sun, Y.W. Yao, R.A. Loomis, W.E. Buhro, Methods for the ICP-OES analysis of semiconductor materials, Chem. Mater. 32 (2020) 1760–1768, https://doi.org/10.1021/acs.chemmater.0c00255.

[5] H.Y. Kim, H.B. Lim, Determination of Si and Cu in Al target metal used in a semiconductor process by inductively coupled plasma-atomic emission spectrometry, Anal. Chim. Acta 429 (2001) 145–150, https://doi.org/10.1016/S0003-2670(00)01236-8.

[6] B.A. Cook, J.L. Harringa, J. Anderegg, A.M. Russell, J. Qu, P.J. Blau, C. Higdon, A. A. Elmoursi, Analysis of wear mechanisms in low-friction AlMgB14-TiB2 coatings, Surf. Coat. Technol. 205 (2010) 2296–2301, https://doi.org/10.1016/j.surfcoat.2010.09.007.

[7] A.M. Grishin, Abrasion resistant low friction and ultra-hard magnetron sputtered AlMgB14 coatings, Mater. Res. Express 3 (2016), https://doi.org/10.1088/2053-1591%2F3%2F4%2F046402.

[8] J. Yang, W. Pan, Y. Han, M. Zhao, M.Z. Huang, C.L. Wan, Mechanical properties, oxygen barrier property, and chemical stability of RE3NbO7 for thermal barrier coating, J. Am. Ceram. Soc. 103 (2020) 2302–2308, https://doi.org/10.1111/jace.16952.

[9] H.F. Chen, C. Zhang, Y.C. Liu, P. Song, W.X. Li, G. Yang, B. Liu, Recent progress in thermal/environmental barrier coatings and their corrosion resistance, Rare Met. 39 (2020) 498–512, https://doi.org/10.1007/s12598-019-01307-1.

[10] A. Limbeck, M. Bonta, W. Nischkauer, Improvements in the direct analysis of advanced materials using ICP-based measurement techniques, J. Anal. Atom. Spectrom. 32 (2017) 212–232, https://doi.org/10.1039/c6ja00335d.

[11] J. Willner, L. Brunnbauer, S. Larisegger, M. Nelhiebel, M. Marchetti-Deschmann, A. Limbeck, A versatile approach for the preparation of matrix-matched standards for LA-ICP-MS analysis - standard addition by the spraying of liquid standards, Talanta 256 (2023), https://doi.org/10.1016/j.talanta.2023.124305.

[12] L. Brunnbauer, Z. Gajarska, H. Lohninger, A. Limbeck, A critical review of recent trends in sample classification using Laser-Induced Breakdown Spectroscopy (LIBS), TrAC-Trend Anal. Chem. 159 (2023), https://doi.org/10.1016/j.trac.2022.116859.

[13] G. Galbács, A critical review of recent progress in analytical laser-induced breakdown spectroscopy, Anal. Bioanal. Chem. 407 (2015) 7537–7562, https://doi.org/10.1007/s00216-015-8855-3.

[14] F. Fahrnberger, M. Siebenhofer, H. Hutter, M. Kubicek, Investigation of atomic-scale decorations on mixed conducting oxides via time-of-flight secondary ion mass spectrometry (ToF-SIMS), Appl. Surf. Sci. 640 (2023), https://doi.org/10.1016/j.apsusc.2023.158312.

[15] D.S. McPhail, Applications of secondary ion mass spectrometry (SIMS) in materials science, J. Mater. Sci. 41 (2006) 873–903, https://doi.org/10.1007/s10853-006-6568-x.

[16] J. Pisonero, B. Fernandez, D. Gunther, Critical revision of GD-MS, LA-ICP-MS and SIMS as inorganic mass spectrometric techniques for direct solid analysis, J. Anal. Atom. Spectrom. 24 (2009) 1145–1160, https://doi.org/10.1039/b904698d.

[17] V. Hoffmann, M. Uhlemann, S. Richter, J. Pfeifer, Calibration capacity of hot-pressed hydrogen standards for glow discharge optical emission and mass spectrometry, Spectrochim. Acta B 176 (2021), https://doi.org/10.1016/j.sab.2020.106039.

[18] G. Friedbacher, H. Bubert, Surface and thin film analysis: a compendium of principles, instrumentation, in: And Applications, 2nd, completely rev. and enlarged ed., Wiley-VCH, Weinheim, 2011 https://doi.org/10.1002/9783527636921.

[19] M. Bonta, J. Frank, S. Taibl, J. Fleig, A. Limbeck, Online-LASIL: Laser Ablation of Solid Samples in Liquid with online-coupled ICP-OES detection for direct determination of the stoichiometry of complex metal oxide thin layers, Anal. Chim. Acta 1000 (2018) 93–99, https://doi.org/10.1016/j.aca.2017.10.025.

[20] M. Podsednik, F. Fahrnberger, D.K. Gibbs, B. Achleitner, S. Larisegger, M. Nelhiebel, H. Hutter, A. Limbeck, Quantitative depth profile analysis using short single pulse responses in LA-ICP-Q-MS experiments, J. Anal. Atom. Spectrom. 39 (2024) 1903–1909, https://doi.org/10.1039/d4ja00082j.

[21] C. Herzig, J. Frank, A.K. Opitz, J. Fleig, A. Limbeck, Quantitative imaging of structured complex metal oxide thin films using online-LASIL-ICP-MS, Talanta 217 (2020), https://doi.org/10.1016/j.talanta.2020.121012.

[22] E.V. Muravitskaya, V.A. Rosantsev, M.V. Belkov, E.A. Ershov-Pavlov, E. V. Klyachkovskaya, Laser ablation in liquids as a new technique of sampling in elemental analysis of solid materials, Spectrochim. Acta B 64 (2009) 119–125, https://doi.org/10.1016/j.sab.2008.11.003.

[23] Y. Tian, A.F. Bastawros, C.C.H. Lo, A.P. Constant, A.M. Russell, B.A. Cook, Superhard self-lubricating AlMgB14 films for microelectromechanical devices, Appl. Phys. Lett. 83 (2003) 2781–2783, https://doi.org/10.1063/1.1615677.

[24] C. Higdon, B. Cook, J. Harringa, A. Russell, J. Goldsmith, J. Qu, P. Blau, Friction and wear mechanisms in AlMgB14-TiB2 nanocoatings, Wear 271 (2011) 2111–2115, https://doi.org/10.1016/j.wear.2010.11.044.

[25] M. Weiss, C. Riedl, J. Frank, J. Fleig, A. Limbeck, Quantitative analysis of the platinum surface decoration on lanthanum strontium iron oxide thin films via online-LASIL-ICP-MS, Microchem. J. 166 (2021), https://doi.org/10.1016/j.microc.2021.106236.

[26] C. Herzig, J. Frank, A.K. Opitz, J. Fleig, A. Limbeck, Quantitative analysis of gadolinium doped cerium oxide thin films via online-LASIL-ICP-OES, J. Anal. Atom. Spectrom. 34 (2019) 2333–2339, https://doi.org/10.1039/c9ja00250b.

[27] M. Podsednik, M. Weiss, S. Larisegger, J. Frank, G. Pobegen, M. Nelhiebel, A. Limbeck, Quantitative analysis of trace elements in technological materials using online-laser ablation of solids in liquids (online-LASIL), Spectrochim. Acta B At. Spectrosc. 205 (2023) 106705, https://doi.org/10.1016/j.sab.2023.106705.

[28] A. Makishima, R. Tanaka, E. Nakamura, Precise elemental and isotopic analyses in silicate samples employing ICP-MS: application of hydrofluoric acid solution and analytical techniques, Anal. Sci. 25 (2009) 1181–1187, https://doi.org/10.2116/analsci.25.1181.

[29] M. Senila, Recent advances in the determination of major and trace elements in plants using inductively coupled plasma optical emission spectrometry, Molecules 29 (2024), https://doi.org/10.3390/molecules29133169.
[30] A. Galuszka, Z. Migaszewski, J. Namiesnik, The 12 principles of green analytical chemistry and the SIGNIFICANCE mnemonic of green analytical practices, TrAC-Trend Anal. Chem. 50 (2013) 78–84, https://doi.org/10.1016/j.trac.2013.04.010.
[31] A.M. Grishin, S.I. Khartsev, J. Böhlmark, M. Ahlgren, Ultra-hard AlMgB14 coatings fabricated by RF magnetron sputtering from a stoichiometric target, Jetp Lett. 100 (2015) 680–687, https://doi.org/10.1134/S0021364014220056.
[32] A. Rabiezadeh, A.M. Hadian, A. Ataie, Synthesis and sintering of TiB2 nanoparticles, Ceram. Int. 40 (2014) 15775–15782, https://doi.org/10.1016/j.ceramint.2014.07.102.
[33] K. Holmberg, H. Ronkainen, A. Matthews, Tribology of thin coatings, Ceram. Int. 26 (2000) 787–795, https://doi.org/10.1016/S0272-8842(00)00015-8.